J. Membrane Biol. 39, 333–367 (1978)

Current-Voltage Relationships for the Plasma Membrane and Its Principal Electrogenic Pump in *Neurospora crassa*: I. Steady-State Conditions

Dietrich Gradmann*, Ulf-Peter Hansen**, W. Scott Long, Clifford L. Slayman, and Jens Warncke

Department of Physiology, Yale School of Medicine, New Haven, Conn. 06510

Received 22 August 1977

Summary. The nonlinear membrane current-voltage relationship (*I–V* curve) for intact hyphae of *Neurospora crassa* has been determined by means of a 3-electrode voltage-clamp technique, plus "quasi-linear" cable theory. Under normal conditions of growth and respiration, the membrane *I–V* curve is best described as a parabolic segment convex in the direction of depolarizing current. At the average resting potential of −174 mV, the membrane conductance is ~190 μmhos/cm^2; conductance increases to ~240 μmhos/cm^2 at −300 mV, and decreases to ~130 μmhos/cm^2 at 0 mV. Irreversible membrane breakdown occurs at potentials beyond this range.

Inhibition of the primary electrogenic pump in *Neurospora* by ATP withdrawal (with 1 mM KCN) depolarizes the membrane to the range of −40 to −70 mV and reduces the slope of the *I–V* curve by a fixed scaling factor of approximately 0.8. For wild-type *Neurospora*, compared under control conditions and during steady-state inhibition by cyanide, the *I–V* difference curve — presumed to define the current-voltage curve for the electrogenic pump — is a saturation function with maximal current of ~20 μA/cm^2, a half-saturation potential near −300 mV, and a projected reversal potential of ca. −400 mV. This value is close to the maximal free energy available to the pump from ATP hydrolysis, so that pump stoichiometry must be close to 1 H^+ extruded:1 ATP split.

The time-courses of change in membrane potential and resistance with cyanide are compatible with the steady-state *I–V* curves, under the assumption that cyanide has no major effects other than ATP withdrawal. Other inhibitors, uncouplers, and lowered temperature all have more complicated effects.

The detailed temporal analysis of voltage-clamp data showed three time-constants in the clamping currents: one of 10 msec, for charging the membrane capacitance (0.9 μF/cm^2); a second of 50–75 msec; and a third of 20–30 sec, perhaps representing changes of intracellular composition.

* *Current address:* Institut für Biologie, Universität Tübingen, 7400 Tübingen, F.R.G.
** *Current address:* Institut für Angewandte Physik, Universität Kiel, 2300 Kiel, F.R.G.

0022-2631/78/0039-0333 $7.00

Over the past 5 years electrogenic pumps (ion transport systems which consume metabolic energy and move net charges through membranes) have been identified in almost all biological membranes examined, so that charge movement has come to be regarded as a basic property of active ion tranport systems. Among those systems which can be studied with direct electrophysiological techniques, the most extensively analyzed is the sodium pump of excitable membranes; however, electrical signals from the sodium pump are customarily small, except during brief periods of rapid transport which may follow potassium-depletion or sodium-loading maneuvers [36, 62], and the role that charge transfer via the sodium pump plays *per se* in the total cellular economy seems small. Quite the opposite is true for electrogenic pumps observed in specialized transporting epithelia [5, 16], as well as for the electrogenic H^+ pumps studied in plant, fungal, and bacterial cells [20, 23, 42] and in mitochondria and chloroplasts [14, 38]. In these cases large membrane potentials, directly associated with active transport processes, are present under steady-state conditions and are postulated to play at least two major roles in the total cellular or tissue economy: that of distributing energy to gradient-coupled transport systems, and that of coupling redox energy to covalent-bond energy [33, 39, 44].

Interest in the electrical properties, *per se*, of active transport systems arises not only out of their contribution to total energy balance in cells, but also out of their implications for the molecular mechanisms of transport. A convenient and widely adopted description of the electrical behavior of membranes — or of membrane constituents — as well as of a wide variety of electronic devices, is the current-voltage plot: a determination of the functional relationship between current flow through the system and the potential difference imposed across the system. Some features of the current-voltage relationship for an electrogenic pump can be predicted from cyclic, enzyme-catalyzed, carrier models containing (i) a voltage-sensitive membrane transit step, and (ii) one or more voltage-insensitive chemical reaction steps (usually represented at each membrane boundary). The latter reactions must become rate-limiting at extreme voltages, so that a maximal (asymptotic) pump current should be observed; it may be regarded as analogous to the maximal velocity for a conventional enzymatic reaction. Furthermore, the total current-voltage relationship for the pump should yield an estimate of the chemical free energy available to the transport reaction, defined by the point at which membrane potential just stops or reverses current flow through the pump. And the detailed shape of the current-voltage curve

necessarily restricts the acceptable classes of molecular models, as is being demonstrated in studies on artificial membranes doped with various passive carriers and "channels" [21, 59].

In the report that follows, we set out the steady-state current-voltage relationship (and some ancillary properties) of the plasma membrane of *Neurospora crassa*, with particular emphasis on the electrogenic H^+ pump in that membrane. Under normal circumstances the pump generates 150–200 mV of membrane potential [41, 51], consumes 25% or more of the total energy available from oxidative phosphorylation [50], supplies energy for concentrative uptake of sugars [53, 54], certain cations [45], and probably amino acids and anions as well [56], and is subject to short-term and long-term control in response to changes in the rate of energy production [18]. It also appears to be driven by hydrolysis of ATP [50, 51], and is probably associated with an ATPase that has recently been identified and partially purified from isolated plasma membranes of *Neurospora* [6, 37]. The new results, of which a preliminary account has already appeared [46], show the current-voltage relationship for the electrogenic pump to be a saturation curve with a maximal velocity close to 20 $\mu A/cm^2$ (200 $pmoles/cm^2 \cdot sec$), an apparent reversal potential near -400 mV, and a half-saturation potential of approximately -300 mV. The detailed current-voltage curve differs significantly from expectation based on existing models for electrogenic pumps and ion carriers [4, 8, 15, 30, 58].

Materials and Methods

General

Except as otherwise noted, experiments were carried out on the wild-type strain RL21a of *Neurospora crassa*. Details of the methods for growing the cells and setting them up for electrophysiological experiments have been reported previously [18, 40]. Briefly, mycelial cultures were grown for 24–40 hr on scratched cellophane supported by 3% agar, at 25 °C. For recording, a section of cellophane with attached mycelium was cut from the agar, rinsed in distilled water, and transferred to a Lucite recording chamber on the stage of a compound microscope. The microelectrodes, reference electrode, solution taps, and vacuum level-regulator were all inserted into the chamber through side ports. All electrical measurements were made at the ambient temperature of 23–24 °C.

Solutions

Cells were grown on Vogel's minimal medium [66] with 2% sucrose, and electrical measurements were made in one of a variety of different buffer solutions, listed in Table 1. Inhibitors were added to these solutions from the following stocks: KCN (J.T. Baker), 100 mM in distilled water, neutralized with HCl; and 2,4-dinitrophenol (DNP, Eastman Kodak), 10 mM in distilled water, neutralized with KOH.

Table 1. Composition of the Media[a]

Ion	Growth medium	Recording solutions concentrations in mM					
		A	B[b]	C	D	E	F[c]
Na	25.3	–	–	–	–	–	7.3
K	36.8	10	25	25	10	10	10.7
NH_4	25.0	–	–	–	1	1	7.2
Ca	0.7	1	1	1	1	1	2.5
Mg	0.8	–	–	–	0.5	0.5	0.23
pH	5.8	5.8[d]	5.8	5.8	5.8	8.2	5.8
Cl	1.4	12	2	2	3	3	5.0
NO_3	25.0	–	–	–	1	1	7.2
SO_4	0.8	–	–	–	–	–	0.23
PO_4	36.8	–	–	23.1	9.1	–	10.7
Citrate	8.4	–	–	–	–	–	2.44
DMG[e]	–	–	20	–	–	–	–
HEPES[e]	–	–	–	–	–	12	–

[a] Traces of biotin and heavy metals were added to all solutions except *A*, *B*, and *C*; also, 1% glucose was added to all solutions except the growth medium, which had 2% sucrose.
[b] NH_4Cl at 1 mM added in some experiments; designated solution B′.
[c] Solution designed to have the same ingredients as growth medium, but a total monovalent cation concentration near 25 mM, with a free calcium concentration (in citrate) of 1 mM.
[d] Unbuffered solution, at the pH of distilled water in equilibrium with air.
[e] DMG = 3,3-dimethylglutaric acid; HEPES = N-2-hydroxyethylpiperazine-N′-2-ethane sulfonic acid.

Electrical Apparatus

The microelectrodes used in these experiments were conventional microcapillary electrodes, filled (by vacuum-boiling at 90 °C) with 3 M KCl. The ground electrode was a 1.5-mm polyethylene tube containing 3% agar and 3 M KCl. All electrodes were connected to the amplifiers through matched Ag-AgCl half cells. Tip junction potentials (tip potentials) were small, approximately −10 mV in most cases, and were therefore neglected. High-impedance electrometer amplifiers ($\doteq 10^{11}$ ohms, leakage current $< 5 \times 10^{-12}$ A; Model M-4, W.P. Instruments) were used to record membrane potentials, usually simultaneously in two adjacent cells of a single hypha. During voltage clamp tests, the amplifier monitoring one cell was connected through a summing network to the negative input of a high-gain operational amplifier (#1545; Burr-Brown, Inc; maximal output ±100 V). The same summing network also led to a variable millivolt source which was used as the clamping command signal. The output of the operational amplifier was connected directly to a second microelectrode, inserted into the same cell of the hypha. The arrangement, with optimal triming capacitance, provided clamp steps from 0 to ±300 mV (referenced to the unclamped membrane potential) having rise times of ca. 3 msec. Performance of the system with depolarizing steps was occasionally degraded by high impedances developed in the microelectrodes during the passage of large outward

currents, but the actual current delivered by the voltage clamp was monitored at the bath ground electrode by an FET electrometer (#310J, Analog Devices) operated as a virtual ground, with a feedback resistor of 10^7 or 10^8 ohms. All signals were displayed on an oscilloscope and a chart recorder.

General Computations and Plots

The earlier experiments reported in this paper (e.g., Fig. 2*A* and *B*) were carried out by manual operation of the voltage clamp, with the data being collected on chart recorders. The data were then transcribed for analysis by hand, or when necessary, for analysis via an IBM 370 computer (Yale Computer Center). Later experiments were carried out with the aid of a Digital Equipment PDP8/E computer, which controlled the voltage clamp and collected data on magnetic tape for subsequent analysis. Curve fitting was done using a reduced version of the Marquardt algorithm [32]. Throughout the paper, average data are designated as mean ± 1 SEM.

Calculation of the Membrane Current-Voltage Curve

Electrically, a hypha of *Neurospora* resembles a complicated, branching, transmission cable, in which the usual distributed parameters — membrane resistance and cytoplasmic resistance — are separated into segments or "cells" by the presence of perforate crosswalls. The effective cross-sectional area of the pores in these crosswalls may be as small as $10^{-3}\times$ the cross-sectional area of the hypha itself, and the pores can be mechanically occluded by nuclei, mitochondria, or small vacuoles in transit, by crystals of ergosterol [40, 64], and (following injury) by a specific closure apparatus [25, 63]. The apparent resistance of the pores is $2\text{–}10\times10^6$ ohms, compared with 4.5×10^5 ohms expected for the axial resistance of the cytoplasm (normal size hyphae: 15 μm diameter, cells 100 μm long); the normal membrane resistance is $1\text{–}5\times10^8$ ohms for each cell. In consequence of these resistance values, current passed from an intracellular microelectrode to a distant external electrode produces a relatively large voltage drop at each crosswall, and a small decrement along the length of any one cell. Therefore, each cell is nearly isopotential, and the hypha as a whole can be treated as a "lumped" transmission cable.

Simplification of the hyphal geometry can be achieved by skewering smaller branch hyphae at some distance from the recording region. This leads to cell death and closure of adjacent crosswalls, and has enabled us to eliminate side branches for a distance of 4–5 cells in both directions from the microelectrodes. Control calculations showed that current flow in the remaining branches creates no more than a 5% error in the apparent membrane current at any voltage, so that such branching was ignored in most of the current-voltage curve determinations. Numerous attempts were made to apply this cell-killing technique along the large stem-hyphae of *Neurospora*, in order to isolate short segments that might be subjected to uniform voltage clamp. Although the maneuver yielded some useful comparative results, summarized in curve 4 of Fig. 5, it ordinarily caused rapid deterioration of the isolated segments and was abandoned for systematic experiments.

Normally, therefore, hyphae were analyzed as one-dimensional lumped cables, with three microelectrodes arranged as shown in Fig. 1. Rectangular voltage pulses were imposed — via the voltage-clamp circuit — on *Cell 0*, and both the input current pulses and the voltage pulses in the adjacent cell (*Cell 1*) were recorded. Three different pulse programs were used, as shown in Fig. 2. Program *A* consisted of 10- to 30-sec pulses, scanning in ca. 30-mV steps over a time interval of 2–4 min; program *B* consisted of slow

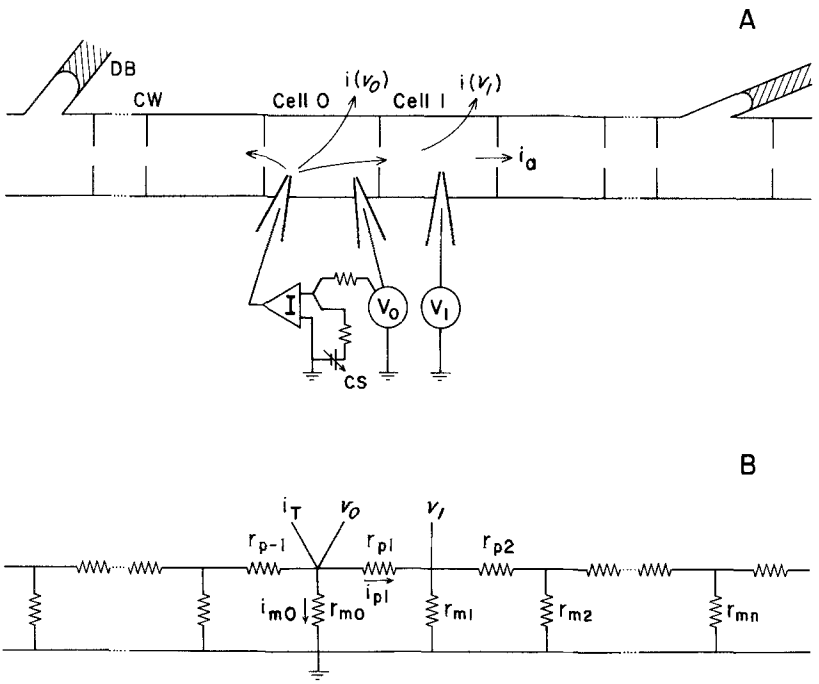

Fig. 1. (*A*): Schematic diagram of a hypha of *Neurospora*, with the standard arrangement of electrodes used for current-voltage curve measurements. (*B*): Equivalent circuit of the hypha, with all resistors treated as finite, lumped parameters. *DB* = dead branch, *CW* = crosswall, *CS* = command signal, r_m = membrane resistance, r_p = pore resistance

ramps or *A*'s with square pulses of ±20 mV superimposed at regular intervals. And in later experiments, a faster computer-controlled scan (program *C*) was adopted. It comprised thirty-two 160-msec pulses, alternating + and − from the resting potential to approximately −300 mV (about 120 mV hyperpolarized) and to 0 mV. Typical plots of input current-voltage data are shown in Fig. 3 for programs *A* (circles) and *C* (squares).

A convenient starting point for derivation of membrane current from measurements of total (input) current is the difference equation for a distributed nonlinear cable, given by Adrian and Marshall [1]. Applying their argument to the lumped cable, for steady-state responses, gives membrane current (i_{m0}; see Fig. 1*B*)

$$i_{m0} = i_T - 2i_{p1} = i_T - \frac{2}{r_{p1}}(v_0 - v_1). \tag{1}$$

If the pore resistance (r_p) were constant, and uniform along the cable ($r_p \equiv r_{p1} = r_{p-1} = r_{p2} \ldots$), it could be evaluated from linear cable theory [41] applied to small pulses (i'_T, v'_1, and $v'_0 \leqq 20$ mV):

$$r_p = \frac{(v'_0 + v'_1)(v'_0 - v'_1)}{v'_1 i'_T}. \tag{2}$$

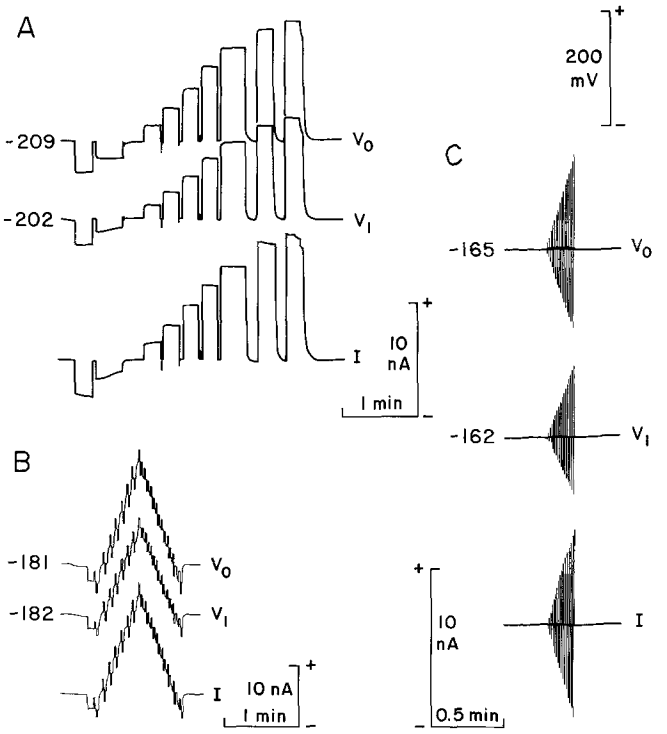

Fig. 2. Records (tracings) from three different *I–V* scans, to illustrate the three types of pulse programs used. V_0, V_1, and *I* designate records for the three electrodes shown in the diagram of Fig. 1*A*. (*A*): 11 to 21-sec pulses, delivered in monotonic order, from −265 mV (at electrode V_0) to 0 mV. Solution B; trial G101. (*B*): 35-sec ramps, from −212 to 0 mV, with superimposed 21-mV pulses. Solution E; trial L24. (*C*): Double train of 160-msec pulses incrementing in 15 steps from the resting potential to −305 and +3 mV. Solution B; trial W319; strain NSX *fa* (*pokyf*). All voltage traces to the same scale, shown upper right. Numbers to the left of each trace are the unclamped membrane potentials

However, calculations of membrane current-voltage relationships via Eqs. (1) and (2) yielded excessively scattered currents, which seemed likely to arise from random fluctuations of r_p. For this reason and also because, in about 25% of experiments, a systematic dependence of r_p on membrane potential emerged (linear decrease in r_p by as much as 30% over the voltage range −300 to 0 mV), we tested a number of alternative procedures. One of these, based on a rigorous nonlinear analysis of the lumped cable, was used for checking and comparison purposes, and is outlined in *Appendix* 2.

In practice, however, the degree of nonlinearity in the *Neurospora* membrane current-voltage relationship has proven small enough that ordinary linear cable theory adequately approximates membrane current, over the testable range of membrane potentials. Substituting Eq. (2) into Eq. (1), dropping the "primes", and consolidating terms, gives

$$i_{m0} = i_T \left(\frac{v_0 - v_1}{v_0 + v_1} \right), \tag{3}$$

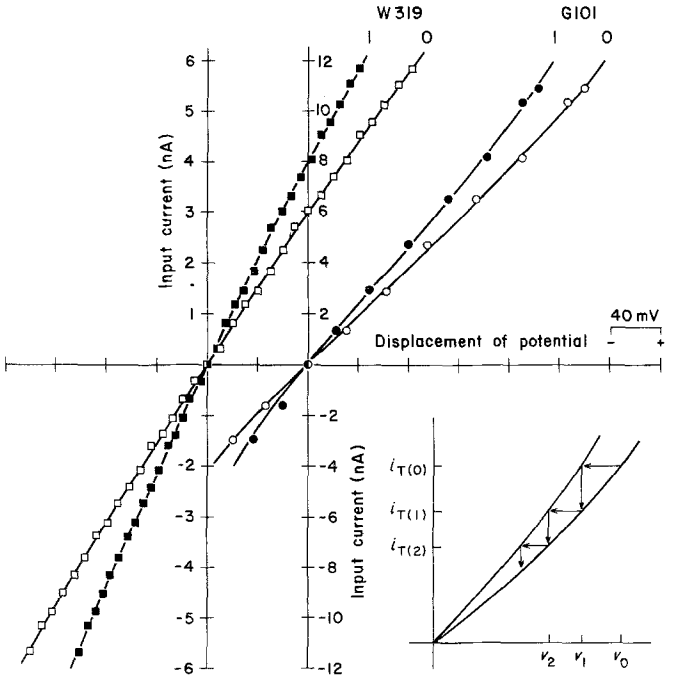

Fig. 3. Input current-voltage plots of the data shown in Fig. 2*A* and *C*. The plotted values were used for calculating membrane *I–V* curves via Eq. (3). Hyphal dimensions, for G101: diameter = 14 μm, cell length = 107 μm; for W319; 9.4 μm and 89.0 μm, respectively. *Inset:* Diagram of the method of stepping off successive voltages and input currents to generate the membrane *I–V* relationship via the nonlinear formula of Eq. (15) *(Appendix 2)*. The smooth curves (main figure) represent 3rd-degree polynomials fitted through the plotted points in order to obtain analytic functions for Eq. (15).

		Polynomial coefficients			
		0^{th}	$1^{st} \times 10^2$	$2^{nd} \times 10^5$	$3^{rd} \times 10^7$
G101,	Cell 0	0	5.05	−5.19	2.23
	Cell 1	0	6.19	−9.89	5.14
W319,	Cell 0	0	3.80	−1.18	−5.43
	Cell 1	0	5.18	−3.00	7.13

which can also be obtained directly from linear theory [41]. In order to evaluate the error in applying this relationship to the nonlinear case, we note that the form of the equation can be preserved for nonlinear cases by introducing two variable parameters, $\alpha = r_{T1}/r_{T0}$ and $\beta = r_{m1}/r_{m0}$, where r_{T1} is the total resistance lying to the right of r_{m1} (Fig. 1*B*). For the linear case, r_{T0} can be written as $0.5(r_p + (r_p^2 + 4r_p r_m)^{0.5})$ [41], $r_{m0} = v_0/i_{m0}$, $r_{p1} = (v_0 - v_1)/i_{p1}$, and $r_{T0} = v_0/i_{p1}$. Combining these with Eq. (1) and the definition of α and β yields, after considerable algebra,

$$i_{m0} = \beta i_T \frac{\alpha v_0 - v_1}{\alpha\beta v_0 + (2\alpha - \beta) v_1}, \tag{4}$$

which approaches Eq. (3) as α and β approach 1. Once a membrane current-voltage curve is obtained via Eq. (3), Eq. (4) can be used — as detailed in *Appendix 1*, to estimate the fractional error in i_{m0}. Typically, the calculated value of $|i_{m0}|$ was found to be 6–7% too small at maximal hyperpolarization and 10–12% too large at maximal depolarization.

Equation (3) has been used for most membrane current calculations in this paper, and the results have been converted to current densities (I_{m0}) by division with the average cell membrane area in the region of hypha under study (i.e., $\pi \times$ hyphal diameter $\times$ distance between successive crosswalls). All membrane current-voltage diagrams have also been translated to the actual values of membrane potential (V_0) in *Cell 0* by adding the resting membrane potential (V_m) to the clamped displacement (v_0): $V_0 = V_m + v_0$. Since a variety of manipulations of the *I–V* curves were required (*see* Figs. 5–9), and since all curves had a common form — with a modest convexity in the direction of the positive current axis, the practice was adopted of fitting the calculated current values as a quadratic function of membrane potential. This procedure is discussed further under *Results*.

Results

The Total Membrane I–V Curve

A necessary strategy for analyzing the relationship of one constituent system within an intact biological membrane is to compare the total membrane *I–V* curves with the system on, and then off. In the case of systems which are rapidly activated and deactivated, as for action potentials in excitable tissues, the data can be obtained as instantaneous or peak currents associated with different clamping potentials in successive on-off cycles. With slower systems, however, a more satisfactory approach is to carry out the entire voltage scan twice (at appropriate times) during a single on-off cycle, and take the difference between the two resultant membrane *I–V* curves. Our first task, then, in approaching the *I–V* curve for the electrogenic pump, was to define the total *I–V* curve for the normal membrane.

Pairs of input current-voltage curves, of the type shown in Fig. 3, were converted via Eq. (3), normalized for membrane area, and translated along the voltage axis to give zero current at the actual resting membrane potential (*see Methods*). The data in Fig. 3 have thus been transformed into the membrane *I–V* curves of Fig. 4 (plotted points). Both of these curves, and almost all others obtained for *Neurospora*, were found to be convex in the direction of positive current, and could be described empirically as parabolic segments. The solid curves in Fig. 4, therefore, are fitted least-squares curves for quadratic equations:

$$I_{m0} = a_0 + a_1 V_0 + a_2 V_0^2, \tag{5}$$

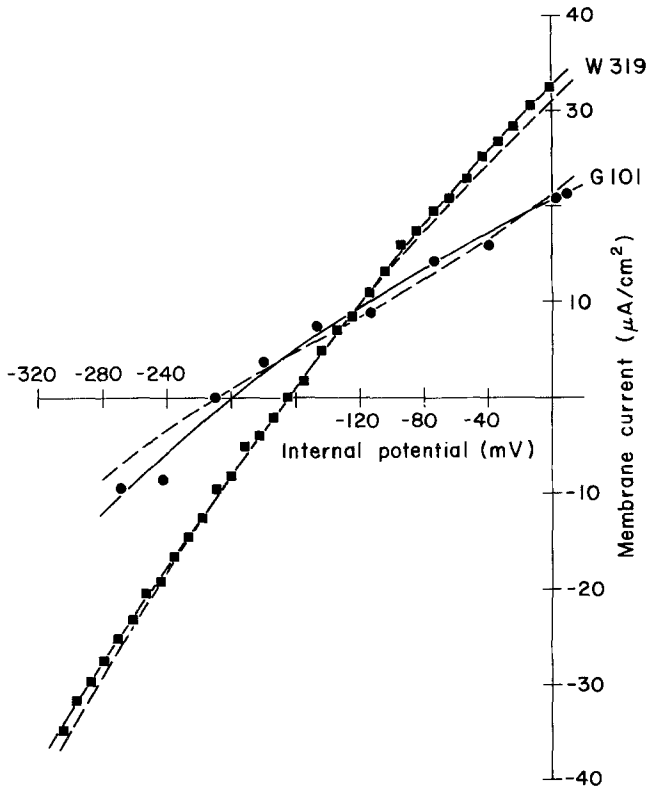

Fig. 4. Membrane current-voltage curves: quasi-linear method checked against nonlinear method. Plotted points calculated by Eq. (3), using individual I and V pulses of Fig. 3. Solid curves are least-squares parabolas fitted through the plotted points. Coefficients [Eq. (5)] in the order of a_o, $a_1 \cdot 10^2$, $a_2 \cdot 10^4$, for G101: 20.0, 6.74, −1.66; for W319: 32.9, 17.6, −1.42. Dashed curves are calculated by Eq. (15), using the fitted curves of Fig. 3

in which the coefficient a_2 describes the voltage-dependence of membrane conductance. (Further improvements of the fit could be obtained by adding third- and fourth-order terms, but the improvements were small (<15%, total) and did not seem to warrant the inflections introduced.)

The dashed curves of Fig. 4 were calculated from the general nonlinear theory for lumped cables (Eq. (15), *Appendix 2*). With high-quality input data (as in W319), Eqs. (3) and (15) give the same membrane I–V curves, within the expected error limits (Eq. (4) and *Appendix 1*). With more scattered input (as in G101), then nonlinear theory tends to produce more complicated curves, but a survey of 25 separate trials showed the additional inflections to be inconstant from one experiment

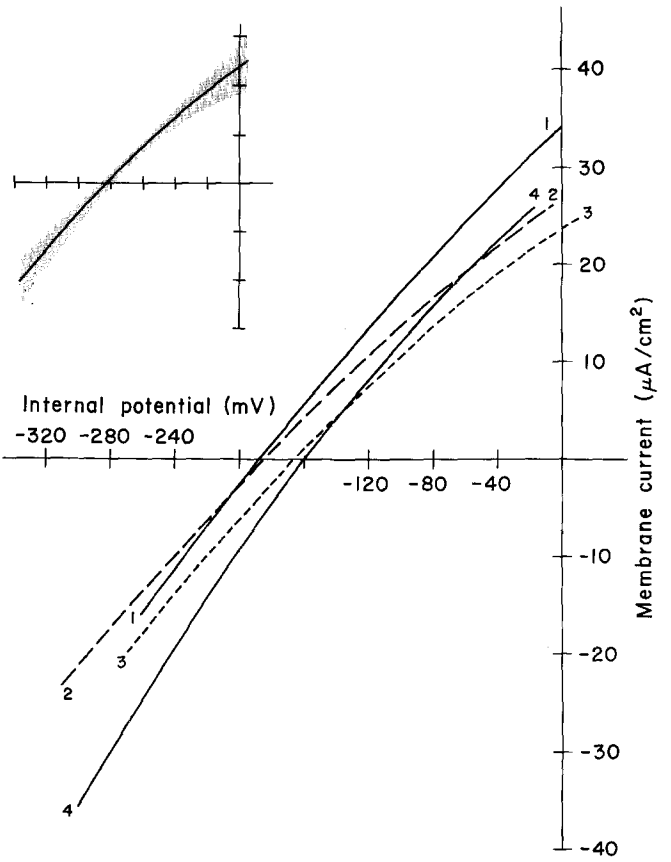

Fig. 5. Synopsis of membrane current-voltage curves. Averages for 4 blocks of experiments; all curves are least-squares parabolas. Values of fitted coefficients, resting membrane potentials, and experimental conditions are specified in Table 2. *Inset:* Curve *3* redrawn, with the stippled area representing ± 1 SEM for each constituent point on the smooth curve

to the next, so that we regard them as spurious. For these reasons, plus the fact that Eq. (3) provides a far more efficient calculating algorithm than Eq. (15), the former was adopted in routine analysis.

The basic shape of the membrane *I–V* curve has been confirmed under a variety of steady-state conditions and with all three pulse programs (*see* Fig. 2). It has also been confirmed in the few successful experiments with isolated short segments of hyphae. In Fig. 5, curve *1* was obtained from slow ramp programs (*B*); curve *2*, from fast pulse programs (*C*); and curve *3*, from slow pulse programs (*A*). Each of these curves is the average result for 5–7 trials on 3–4 hyphae. Their separation should be compared with the spread of individual *I–V* curves, described by the stippled region

Table 2. Numerical results for Fig. 5

Curve #	1	2	3	4	Averages
Medium used (from Table 1)	A, D	B′	B	F	
#Trials/#Hyphae	5/4	7/3	6/4	6/2	
Fitted coefficients [Eq. (5)]					
a_0	34.4	26.8	23.0	28.3	–
$a_1 \times 10^2$	15.8	11.9	11.2	13.7	–
$a_2 \times 10^4$	−1.34	−1.37	−1.85	−2.55	–
Σd^2 [a]/#points	2.0/18	0.9/32	5.6/10	7.8/30	–
Resting potential V_m (in mV)	−188±6	−185±6	−166±8	−159±1	−174±4
Slope conductances G_m (in μmhos/cm^2)					
at −300 mV	239	201	223	290	238±19
V_m	209	170	173	218	192±12
0 mV	158	120	112	137	132±10

[a] Quadratic coefficients were chosen to minimize Σd^2, the squared deviation between the average "observed" membrane current and that calculated via the quadratic equation.

(±1 SEM) of the inset drawing in Fig. 5. Curve *4* is the average result for 6 trials on 2 isolated hyphal segments 300–400 μm long, for which membrane current was calculated simply as the quotient of the total current and the total membrane area of each segment. (This calculation produces a small scaling error along the voltage axis, since the segments were too long to be truely isopotential; voltage displacement at the ends should have been 10–15% smaller than near the current microelectrode.) The ensemble of curves in Fig. 5 demonstrate that the steady-state membrane current-voltage curve of *Neurospora* is insensitive to culture conditions (*see* Table 2), to the duration or pattern of scanning pulses, and to the history of punctures and crosswall closures (provided the hypha or hyphal segment survives). Curve *4* — obtained from surviving short segments — validates the determination of membrane *I–V* curves on intact (debranched) hyphae.

Essential descriptive parameters for the curves in Fig. 5 are provided in Table 2. The average slope conductance of the membrane at the resting potential, 192 μmhos/cm^2, is identical with that previously calculated from small pulse data [41]. As is to be expected from curves described by Eq. (5), membrane conductance shifts symmetrically with

hyperpolarization or depolarization; and it decreases by about half between −300 and 0 mV. The ramp-and-pulse program (*B*) used to generate data for curve *1* also provided data for an independent calculation of membrane slope conductance. The mean amplitude of the small voltage-clamp pulses for the 6 experiments was ±22.3 mV, and the current required to produce this displacement decreased from 5.8 μA/cm² at −300 mV to 3.9 μA/cm² at 0 mV, which translates — from the derivative of Eq. (5) — into $a_2 = -1.66(\pm 0.18) \times 10^{-4}$ and $a_1 = 17.5 (\pm 0.5) \times 10^{-2}$. The value of a_2, the voltage-dependence parameter for membrane conductance, does not differ significantly from that in curve *1*; a_1, the conductance at 0 mV, does differ from the value in curve *1*, but

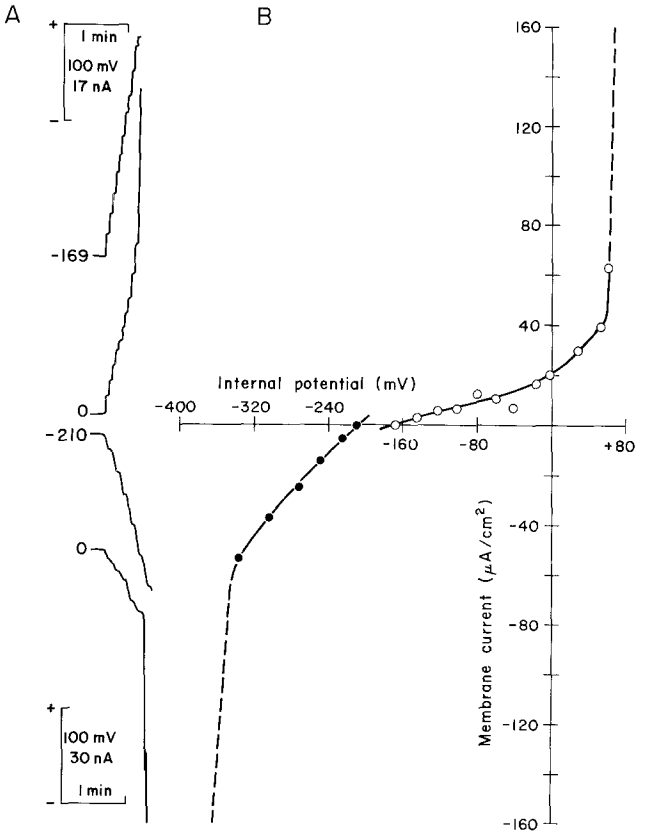

Fig. 6. Membrane breakdown during current-voltage scans to extreme voltages. (*A*): Voltage and current traces for depolarizing trial (upper pair) and hyperpolarizing trial (lower pair), on separate hyphae. (*B*): Calculated membrane *I–V* relationship [Eq. (3)] from the matched steps in *A*, plus V_1 data (not shown). Open circles (○), depolarizing; filled circles (●), hyperpolarizing. *Upper:* Hypha L33; diameter = 19.3 μm, cell length, 115 μm. *Lower:* L34; diameter = 14.4 μm, cell length, 82 μm. Solution C throughout

70% of the difference can be accounted for by resetting errors in the chart recorders.

Voltage scans throughout these experiments have been limited to the range −300 to 0 mV for three reasons: (i) excessive scatter in the current data with polarization outside that range; (ii) unpredictable jumps in axial resistance with very large currents and (iii) occurrence of irreversible membrane damage by −350 or +70 mV. Current and voltage data from two such breakdown experiments are shown in Fig. 6. In these cases clamping current became uncontrollable at +60 mV (upper half figure) and at −335 mV (lower half). The depolarizing curve, furthermore, showed an increase of membrane conductance at positive membrane potentials, prior to breakdown. Whether this behavior is general or only occasional for *Neurospora* is not known, but it has also been seen with giant algal cells [9, 17].

Current-Voltage Relationship for the Electrogenic Pump

The problem of obtaining pump *I–V* curves now reduces to that of switching the pump off and repeating the procedures used in Figs. 4 and 5 above. Unfortunately, no specific inhibitor (such as ouabain, for the sodium pump in animal cell membranes) is known for the plasma membrane H^+ pump in fungi, algae, or bacteria. This necessarily means that switching must be done with more general inhibitors, and the simplest one in the case of *Neurospora* seems to be cyanide. KCN, at 1–3 mM, blocks ca. 98% of respiration in the wild-type strain [29], with subsequent depolarization of the plasma membrane [50, 51] and cessation of growth [55]. ATP depletion occurs with a simple exponential time constant of 6 sec (25 °C), and — after a 3- to 4-sec lag — is closely tracked by membrane depolarization [50]. Time courses of depolarization with cyanide show no clear second component, contrary to earlier expectations [47, 48], and we have adopted cyanide treatment of wild-type *Neurospora* as the best means presently available to inhibit the electrogenic pump.

The actual operation of extracting a pump *I–V* curve is illustrated in Fig. 7. The total membrane *I–V* curve was determined 1–3 min before addition of cyanide, after 0.5–5.0 min in cyanide, and again several minutes after washout of cyanide (by which time the membrane potential had recovered to the control value). The "before" and "after" plots were fitted to a common parabola, from which was then subtracted the

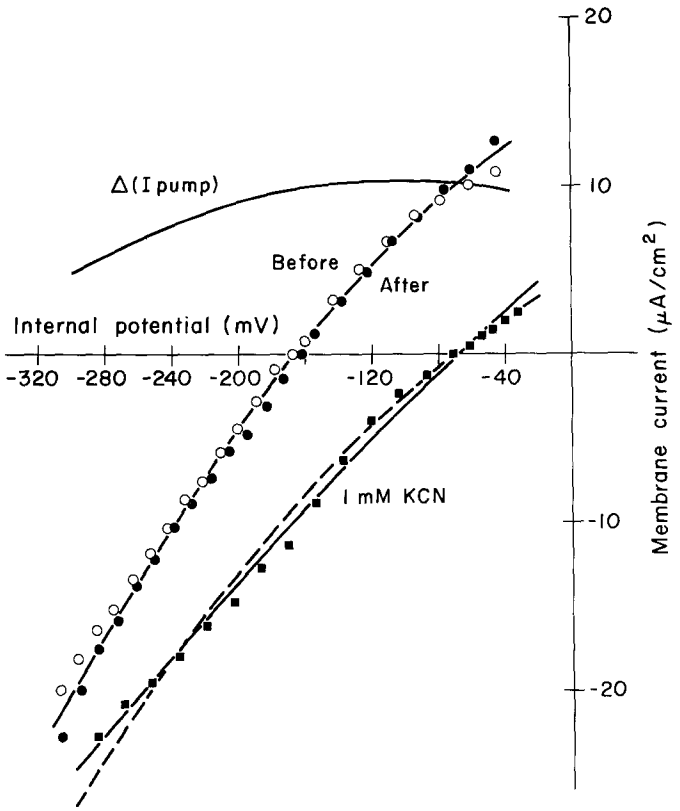

Fig. 7. Generation of a current-voltage curve for the electrogenic pump. Points calculated from individual *I* and *V* pulses, via Eq. (3). *Middle curve:* Common least-squares parabola for the control (○) scanned 1 min before addition of cyanide, and the wash curve (●) scanned 6 min after removal of cyanide. *Lower solid curve:* The least-squares parabola for the membrane *I–V* plot (■) scanned in 1 mM KCN (1 min). *Upper curve:* Difference of the two membrane *I–V* curves.

	Polynomial coefficients		
	a_o	$a_1 \cdot 10^2$	$a_2 \cdot 10^4$
Before/after	14.8	5.41	−2.07
KCN	6.01	8.45	−0.63
Δ	8.77	−3.04	−1.44

Solution B, ±1 mM KCN throughout. Resting membrane potentials: −169/−163 mV without cyanide, −72 mV in cyanide. Cell dimensions: 17.2 μm diameter, 98.9 μm length. *Lower dashed curve:* Curve drawn by the "proportional slope" method described in *Appendix 3*

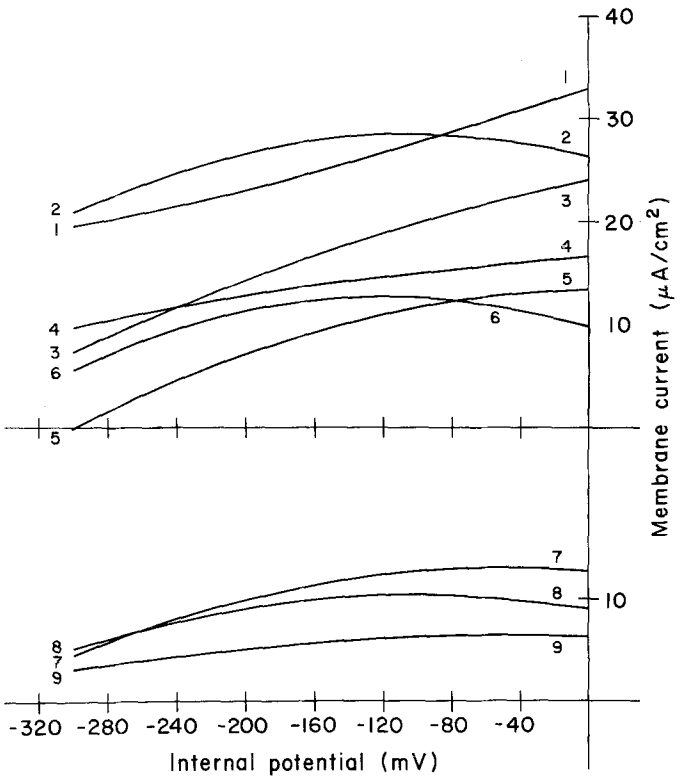

Fig. 8. Summary of pump current-voltage curves. Each curve was obtained in the manner developed in Fig. 7 (curve *8* is a redrawing of the upper curve in Fig. 7). Values of quadratic difference coefficients, resting membrane potentials, and experimental conditions are listed in Table 3

parabola fitted to the "during cyanide" plot (lower plot, solid curve). (The dashed curve here is discussed in *Appendix 3*.) In the example of Fig. 7, the difference curve showed a pump current of about 5 $\mu A/cm^2$ at -300 mV, which rose to about $10\,\mu A/cm^2$ near -140 mV, and was roughly constant with further depolarization.

A summary of our nine most reliable pump *I–V* curves is provided in Fig. 8 and Table 3. All curves share a common feature of shape in the decline of current with membrane polarization negative to about -100 mV, but only one (curve *5*) actually reaches zero current, defining the reversal potential within the range of achievable membrane potentials. Four curves (Nos. *3*, *6*, *7*, *8*) extrapolate to zero current at potentials positive to -400 mV, and the rest (Nos. *1*, *2*, *4*, *9*) might best be described as quasi-current sources, which do not convincingly extrapolate to zero current. Such results, taken by themselves, would not

Table 3. Numerical results for Fig. 8

Curve #	1	2	3	4	5	6	7	8	9
Hypha #	W273	L13	W213	W281	G101	L72	G111	W221	W485
Medium used (from Table 1)	B	D	B	B	B	E	B	B	B′
Pulse program (from Fig. 2)	C	B	C	C	A	B	A	C	C
Fitted coefficients [Eq. (5)]									
a_o	33.0	26.3	24.1	16.6	13.3	9.56	12.7	8.77	6.31
$a_1 \times 10^2$	5.76	−4.13	3.62	1.26	0.301	−5.13	−1.29	−3.04	−0.360
$a_2 \times 10^4$	0.418	−1.99	−0.662	−0.351	−1.40	−2.16	−1.34	−1.44	−0.472
Resting potential V_m (in mV)									
control (aver)	−167	−171	−195	−177	−189	−198	−167	−166	−173
in cyanide	−62	−79	−112	−63	−71	−89	−42	−72	−64

admit a clear interpretation. However, extensive studies on the *poky f* strain of *Neurospora* under various conditions of metabolic adaptation[1] have indicated that the apparent reversal potential for the electrogenic pump can shift out of and into the measurable range (sometimes reaching as low as −200 mV), depending on the metabolic state of the cells. It seems reasonable, therefore, to look upon the scatter in shapes of pump *I–V* curves in Fig. 8 as reflecting smaller shifts of this kind in the wild-type strain.

The average pump *I–V* curve for all 9 cases described above is shown as the plotted points in Fig. 9, with ±1 SEM at each point given by the stippled area. The solid curve drawn through the points represents a simple exponential function, translated along the voltage axis to the (best fit) reversal potential:

$$I_{\text{pump}} = I_{\max}(1 - e^{-(V_0 - E_p)/\varepsilon}), \tag{6}$$

where $I_{\max}$ is the current asymptote at strong depolarization, E_p is the apparent reversal potential, and the half-saturation potential is defined by $E_p + 0.69\,\varepsilon$. Least-squares estimates for the parameters were obtained via the Marquardt algorithm [32], and confidence limits were obtained

1 Warncke, J., Gradmann, D., Slayman, C.L. *(manuscript in preparation).*

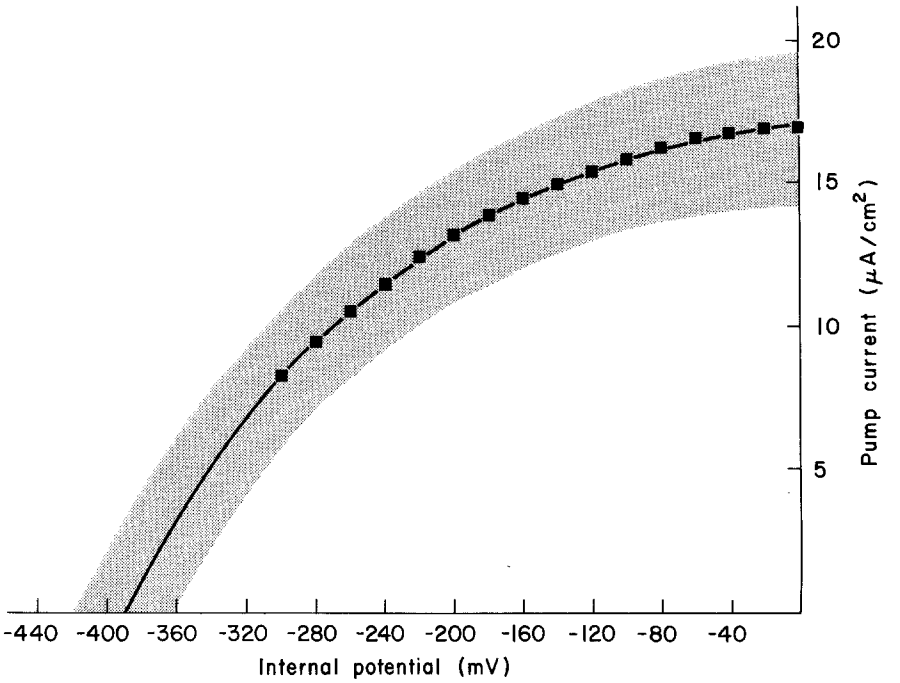

Fig. 9. Average pump current-voltage curve. The plotted points (■) are averaged values for the 9 curves in Fig. 8 with ±1 SEM shown by the stippled region. The solid curve is a single exponential [Eq. (6)], fitted by least-squares, with $E_p = -390 \pm 29$ mV, $I_{max} = 18.6 \pm 3.3$ μA/cm² and $\varepsilon = 153 \pm 23$ mV

by fitting Eq. (6) to the upper and lower boundaries of the stippled region: $E_p = -390 \pm 29$ mV, $\varepsilon = 153 \pm 23$ mV, the half-saturation potential is -284 ± 33 mV, and $I_{max} = 18.6 \pm 3.3$ μA/cm². Since cyanide inhibition does not exhaust intracellular ATP nor completely block the electrogenic pump [50], but leaves residual pumping roughly equal to 25% of the uninhibited steady-state rate, the true maximal pump velocity is probably near 25 μA/cm².

Interpretation of Simple Membrane Conductance Measurements

In the classical studies of excitable tissues, a great deal of information has been gleaned from simple measurements of membrane slope conductance obtained, e.g., by imposing small current pulses and observing the voltage displacements. Such measurements are attractive because they are simple to make and can be used to follow membrane events more or less continuously. However, when dealing with membranes

whose electrical properties are intimately related to metabolism – rather than largely buffered by ion-diffusion regimes – such measurements are likely to be misleading without detailed knowledge of changing membrane current-voltage relationships. At best, simple conductance measurements can only be used to test for consistent behavior of the membrane under various circumstances, with respect to a known type of I–V relationship.

The simple question might be asked, whether the *time-course* of membrane conductance change during cyanide inhibition is consistent with membrane and pump current-voltage relationships deduced from the steady-state I–V curves. The answer to this question, a qualified "yes", is illustrated in Fig. 10. There, average conductance (A) and voltage (B) data are plotted for two consecutive cyanide trials (20 min apart) on a single hypha. Membrane conductances were estimated using the linear cable relation $G'_m/G_m=(v_0/v'_0)^2$ [41] from responses to fixed small current pulses (4×10^{-9} A). In the absence of explicit I–V curve determinations over the whole time-course of depolarization, the expected slope conductance corresponding to each value of membrane potential can be estimated from the empirical finding that I–V curves during cyanide inhibition (of wild-type *Neurospora*) are similar in shape to the control curves, but with a scaled-down slope and depolarized voltage intercept. The general method is outlined in *Appendix 3*, and leads to the following equation relating the membrane conductance ($G_{m0}(t)$) at any time during cyanide inhibition to the unclamped membrane potential ($V_{m0}(t)$) at that same time:

$$G_{m0}(t)=\frac{(a_2E_p^2+a_1E_p+a_0)(2a_2V_{m0}(t)+a_1)}{a_2(E_p^2-V_{m0}^2(t))+a_1(E_p-V_{m0}(t))}. \tag{7}$$

(In fitting this equation to the data in Fig. 10, only a single parameter, a_2, was optimized; a_1 and a_0 were calculated from a_2 plus the control membrane potential and conductance (-159 mV, 187 μmhos/cm^2), and E_p was assigned a value, -418 mV, slightly negative to the average reversal potential for the pump (*see Appendix 3*).) The implied control membrane I–V curve is plotted in the inset to Fig. 10, and lies well within the range of shapes expected from Fig. 5.

The actual fit of Eq. (7) to the conductance data shows general agreement, with two discrepancies: (i) membrane conductance undergoes a small initial rise, prior to the onset of depolarization, and (ii) the data cross the fitted curve at about 100 sec. The former behavior has often

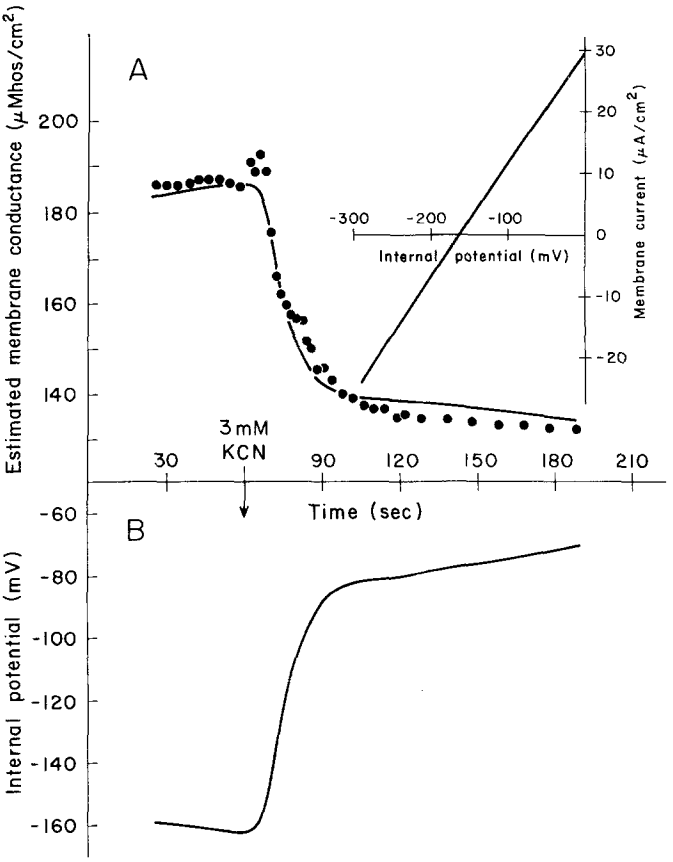

Fig. 10. Test of the ability of steady-state I–V analysis to describe time-dependent change of membrane conductance at onset of cyanide inhibition. Two-electrode experiment, with I and V_0. Membrane conductance estimated, assuming longitudinal resistance to be constant, from the square of the input conductance [41], and scaled to give 187 μmhos/cm² at beginning of plot (expected for a resting potential of −159 mV; *see* Table 2). (*A*): Conductance plot (●), with Eq. (7) fitted by optimizing only parameter a_2 (solid curve), and constraining E_p to be −418 mV *(see Appendix 3)*. Four points at 62–68 sec omitted from the fit. (*B*): Voltage trace from record on which test pulses were superimposed. *Inset:* Control membrane I–V curve implied by the fitted curve of part *A*; a_2 found to be -0.343×10^{-4}, $a_1 = 17.5 \times 10^{-2}$, $a_0 = 29.4$. Hypha G172, solution B

been observed during cyanide treatment, and is of unknown origin. The latter behavior arises from a conductance "notch" at approximately the time (20 sec) required for activation of a metabolic control system which brings about membrane repolarization in the *poky f* strain of *Neurospora* [18]. That control system appears to operate only abortively in normal wild-type *Neurospora*, as will be discussed in a subsequent paper [2].

2 *Ibid.*

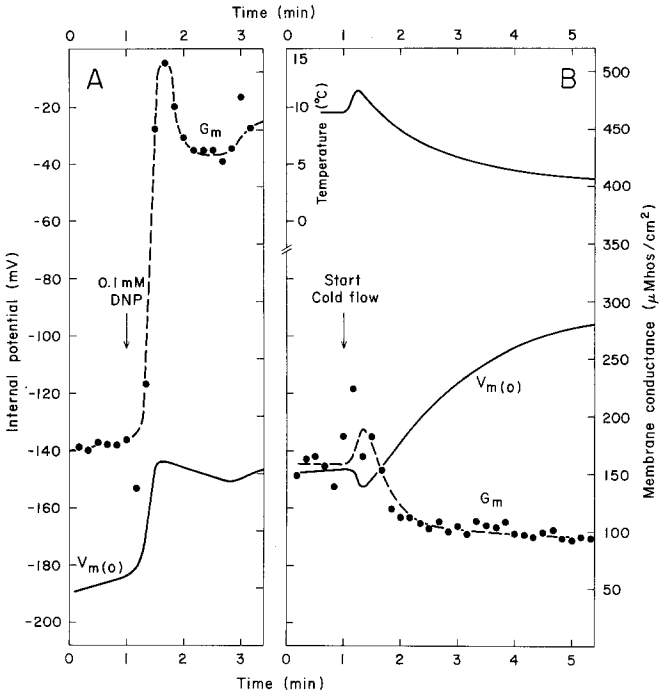

Fig. 11. Disproportionate changes of membrane conductance and potential for two other inhibitors. (*A*): 0.1 mM 2,4-dinitrophenol (DNP). Strain NSX *fa* (*poky f*), hypha G182, solution C. (*B*): Cooling; top trace is temperature measured with a microthermocouple placed next to the hypha. Wild-type strain RL21*a*, hypha S168, solution B. Conductance data for *A* obtained as described in Fig. 10; for *B*, actual membrane conductance was calculated from data at three microelectrodes. Note large increase of conductance and small depolarization with DNP; and relatively fast decrease of conductance with temperature change

Inhibitors other than cyanide yield quite different relationships between membrane potential and membrane conductance. For example, low concentrations (10–100 μM) of DNP (Fig. 11*A*) *elevate* membrane conductance two- to threefold, but depolarize only slightly (by 30–60 mV); and small temperature downshifts (Fig. 11*B*: 9.6→3.6 °C) depress membrane conductance, but with a time-course that is quite different from the time course of membrane depolarization. It is clear that the membrane response to these inhibitors is not compatible with simple deactivation of the electrogenic pump – as defined by cyanide treatment – and must involve more complex changes of the membrane current-voltage relationship.

Multiple Time-Constants in the Current- and Voltage-Pulse Data

Throughout the above presentation, the tacit assumption has been made that the measured current and voltage pulses were of similar shape, without transients which would violate the steady-state assumption built into Eq. (1)–(4). Three types of transients were, in fact, observed which shed interesting light on the circumstances of measurement. Fortunately, only one of these transients introduces error (small) into the *I–V* curve calculations.

1) *Current-dependent voltage drift.* With the slow pulse program (*A*), a systematic drift of the (unclamped) resting membrane potential was sometimes observed, as illustrated in Fig. 12*A*. In the case shown it amounted to a maximal 24-mV depolarization associated with depolarizing pulses of 140 mV, and a maximal 12-mV hyperpolarization with hyperpolarizing pulses of 80 mV. The phenomenon has not been explored in detail, but may well arise from local changes of cytoplasmic composition, as the following calculation will show. The electrodes were inserted into an isolated hyphal segment 215 μm long and 15 μm in diameter. The total (+) charge injected into the segment to reach peak depolarization was approximately 300 nC = 3 pmoles, which – in a volume of 3.8×10^{-8} cm^3 – would represent a total concentration of 80 mM for an unbuffered species (e.g., K^+ or Cl^- carrying current through the microelectrode). If membrane current were carried predominantly by protons, then an alkaline shift of cytoplasmic pH by 1.5 units would have been expected, based on a previous determination of cytoplasmic buffer capacity [52]. Such a pH shift should both alter the diffusion component of membrane potential and modulate the electrogenic H^+ pump. (There is no obvious way to account for the failure of the V_m change in Fig. 12*A* to peak at maximal hyperpolarization.)

No hyphae showing this kind of voltage drift were used for *I–V* curve calculations.

2) *Membrane capacitance.* Detailed examination of currents and voltages with the fast pulse program (*C*) revealed two additional events. A typical example of the pulse data is shown in Fig. 12*B*, where the plotted points represent computer readings averaged (internally) over 32-msec intervals. (The slight overshoot with most voltage steps is an artifact.) The most conspicuous feature of these plots is the substantial current transient observed at every step. Although the computer program was not designed to give a detailed time course for this transient, it almost certainly represents charging of membrane capacitance. By triangular approximation (dotted lines), the total excess charge flow (q_T) was

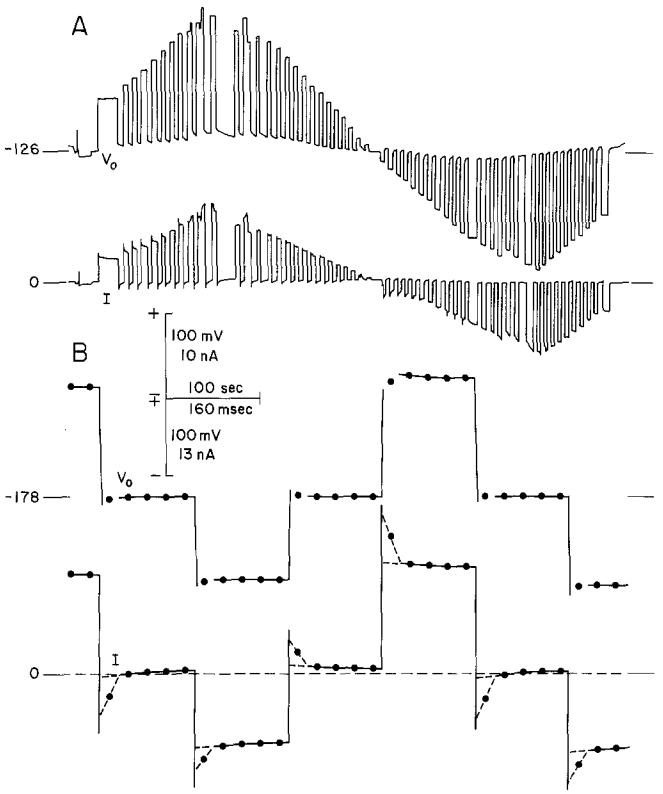

Fig. 12. Time constants in the current- and voltage-pulses. (*A*): Chart records from an isolated segment, studied with long pulses (program *A*). Note drift of the resting membrane potential (clamp off), roughly proportional to amplitude of polarizing pulses; also, gradual relaxation with duration of clamp off. Sharp peaks on current record are artifacts. Hypha G205, diameter = 15 μm, length = 215 μm; solution B. (*B*): Plots of computer data from hypha studied with pulse program *C*, to show charging of membrane capacitance and possible unstirred-layer effect (current relaxation). Hypha H292, diameter = 24.5 μm, cell length 270 μm; solution F without sugar. Carbon-starved hypha. *See* Table 4 for summary of results from this figure

126 *pC*, 77, 86, 148, 138, and 101 *pC*, respectively, for the six transients plotted; the corresponding voltage displacements were 146 mV, 90, 91, 156, 156 and 115 mV. Thus, total measured capacitance of the hypha averaged 0.9 nF. The membrane *I–V* relationship for this particular hypha was essentially linear, and in that circumstance membrane capacitance is related to total capacitance by the same factor (*see* Eq. (3)) as membrane current is related to total current:

$$c_m = \frac{v_0 - v_1}{v_0 + v_1} \cdot \frac{q_T}{v_0}. \tag{8}$$

Table 4. Second-order effects of I–V pulses

Amplitude	Time constant	Origin
$1pC$/mV	10 msec	membrane capacitance
$0.1 \times I$	50–75 msec	extracellular unstirred layer? internal charge relaxation?
$0.15 \times v_0$	20–30 sec	cytoplasmic Δ pH?

For the pulses in Fig. 12*B*, v_0 averaged 126 mV and v_1 (not shown) averaged 82 mV, so that $c_m = 0.9\,\text{nF} \times 0.21 = 0.19\,\text{nF/cell}$. Cell length and diameter were 270 μm and 24.5 μm, respectively, making $C_m = 0.91$ μF/cm^2. (This figure might be adjusted upward 5–10% to accomodate the error in calculating q_T by triangular approximation.) The slope resistance of the membrane was 10 kohm · cm^2, so the time constant was 9–10 msec.

Computation of pulse amplitudes for the I–V calculations always excluded the first averaging interval (0→32 msec), so that capacity charging was 95% complete. The residual charging current is subsumed in the slower transient described below.

3) *Current drift.* Following each capacitative transient was a small current relaxation having a time constant of 50–75 msec and an amplitude (0.6–1.2 nA, for the data in Fig. 12*B*) roughly proportional to the pulse amplitude. Since it occurred at both pulse-on and pulse-off, it could reflect a change in membrane voltage, but not a change in membrane resistance. Though this current drift is in the same direction as that discussed for Fig. 12*A*, its speed makes it unlikely to arise from variations of cytoplasmic composition. It probably arises either from current-flow through an extracellular unstirred layer or from charge relaxation within the membrane [10].

Pulse currents used for I–V analysis were calculated as the average of the last four values in each pulse. This introduces approximately a 6% scaling error into the membrane currents (calculated currents smaller than would have been observed for a brief pulse at 0 msec).

Table 4 summarizes the three different time-constants found in the pulse data.

Discussion

The membrane current-voltage relationship of *Neurospora* differs from that of the well-characterized giant algal cells [13, 57] in displaying a longer region of upward convexity (along the positive current axis),

although we have not yet systematically explored the effects of changes in ionic strength, divalent cation level, or external pH. The steep increase of current with polarization beyond −350 mV (Fig. 6) is reminiscent of ionic "punch-through" observed with *Chara* and *Nitella* [9], but its irreversibility in the case of *Neurospora* suggests that it is more akin to capacitative breakdown than to true punch-through. There is no plausible explanation for the apparently similar breakdown seen at small positive membrane potentials in *Neurospora*, but the foot of the rising curve (Fig. 6) may be analogous to the rising potassium-current characteristic reported for the depolarized plasmalemma of *Acetabularia* [17]. Under certain, as yet ill controlled, circumstances with *Neurospora*, the inflection point may shift to negative potentials, thus permitting sluggish "action potentials" to occur during physiological depolarization [49].

There are probably three major components in the total membrane *I–V* curve of normal, wild-type *Neurospora*: the electrogenic H^+ pump, ion-dependent substrate cotransport systems, and passive ion movements. Only the first of these is broached by the present results. The average pump *I–V* curve obtained for *Neurospora* yields three characteristic parameters which must be accounted for by any model of the pump: a maximal current, $I_{max} = 18.6\,\mu A/cm^2 \rightarrow 25\,\mu A/cm^2$ (*see* discussion of Fig. 9); the voltage characteristic, $\varepsilon = 153\,mV$; and the apparent reversal potential, $E_p = -390\,mV$. (The choice of Eq. (6) to fit the data of Fig. 9 was based on expectation from various theoretical models [4, 8, 15, 30, 58]. It must be emphasized, however, that actual values for the parameters are rather insensitive to the exact saturation function chosen. With a rectangular hyperbola, for example, optimized parameters are 23.5 $\mu A/cm^2$, 136 mV, and −374 mV, in the same order as above.) The significance which can presently be attached to each of these parameters is considered below.

Reversal Potential

The membrane potential which just balances the driving force of the pump, and stops current flow, can be derived independently of the specific models for the pump, and is simply

$$E_p = \frac{RT}{zF}\left[\ln K_{ATP} + \ln \frac{[ATP]_i}{[ADP]_i \cdot [P_i]_i} + z \cdot \ln \frac{[H^+]_i}{[H^+]_o}\right], \tag{9}$$

where K_{ATP} is the equilibrium constant for ATP hydrolysis, and the square-bracketed terms are concentrations (intracellular (*i*) or extracellular (*o*)). Each cycle of the pump is assumed to consume 1 molecule of

ATP and to transfer z ions of H^+, and the hydrolysis reaction is assumed to take place without itself creating protons (pH 6.2–6.5, from Refs. [3], [60]). The total energy available from ATP hydrolysis under normal conditions for *Neurospora* was previously calculated to be 12 kcal/mole, or 520 mV [50]; internal pH was also estimated to be 6.5 [52], compared with an external pH of 5.8 in the present experiments, which would subtract about 40 mV in Eq. (9). Thus, with a single H^+ ion transported outward for each cycle of the pump ($z=1$), the reversal potential should be near -480 mV. The facts that the average reversal potential from Fig. 9 is as large as $(-)$ 390 mV and that nearly half the pump I–V curves clearly do not extrapolate to zero current until well beyond that value imply that the normal ratio, H^+ transported/ATP split, must indeed be close to 1.

It seems unlikely that variations of cellular nucleotides or pH_i could be large enough to account for the lowest measured value of E_p, -299 mV for curve 5 of Fig. 8, and we tentatively favor the interpretation that transport stoichiometry can change, with z shifting toward 2 under certain conditions. A more detailed analysis of this point will be given later[3], but it should be noted here that the phenomenon is also discernable in the conductance plot of Fig. 11*A*. In that experiment 0.1 mM DNP produced a 40-mV depolarization, with a threefold increase of membrane conductance. A rough equivalent circuit analysis of the situation [46] made clear that pump conductance, in addition to leak conductance, increases under the influence of DNP. This means that the I–V relationship for the pump must get steeper near the resting potential, as if the whole I–V curve (in Fig. 9) were shifted rightwards, with the reversal potential moving toward the resting membrane potential. (Such a result evokes findings on energy-conserving membranes, where DNP binds to ATPases and strongly influences their affinity for adenine nucleotides [19, 26].) The general idea of variable pump stoichiometry is consistent with earlier evidence on the behavior of the Na^+/K^+ pump in striated muscle [2, 12] and with reports on proton-driven cotransport systems in algae and bacteria [27, 35].

The Voltage Characteristic

This parameter, along with I_{max}, is necessarily defined only for transport models which in fact show saturation as a function of voltage;

3 *Ibid.*

i.e., models in which voltage-insensitive steps, either chemical reactions at the membrane interfaces or transit of uncharged carrier forms, become rate limiting for the overall transport process. A peculiar feature of the pump *I–V* curves shown in Figs. 7–9 is the large value of ε, which means the large voltage spread occupied by the transition between zero current and saturating current. Most carrier models predict values for ε in the range 25–50 mV [4, 8, 30], and the ion pump system in *Acetabularia* shows values varying from 10 to 50 mV [17]. For the electrogenic pump in *Neurospora*, the average value of ε is more than 150 mV, and the difference from above mentioned values is far outside the range of experimental error. Two different kinds of explanation seem possible: (i) Voltage-sensitive and voltage-insensitive steps in the overall transport cycle are not clearly separated, either because binding and transit into the membrane define a single activation process, or because the interfacial reactions are somewhat voltage sensitive. (ii) ε does not characterize a single type of transport reaction, but is the average of two: one for $z=1$, and another for $z=2$, each of which could have a much smaller voltage characteristic. If, under any given set of circumstances, some pumps in the membrane use each reaction, then the population average should show a voltage-dependent segment which spans between the two reversal potentials. This interpretation must play a role if the concept of variable pump stoichiometry is correct in the present context.

The maximal conductance of the electrogenic pump (G_{max}) is given by the slope of the *I–V* curve at zero current, and is simply I_{max}/ε. From the parameter values listed above, $G_{max}=122$–$163\ \mu mhos/cm^2$, which compares with an extrapolated total membrane conductance at -390 mV of about $350\ \mu mhos/cm^2$ (average value for Fig. 5 and Table 2; not considering the breakdown phenomenon of Fig. 6), so that the pump would account for 35–47% of the total. At a resting potential of -175 mV (*see* Tables 2 and 3), $G_{pump}=30$–$40\ \mu mhos/cm^2$, or only 15–20% of the total membrane conductance. This latter figure accounts for the observation (*see* Fig. 10*A* above and Ref. 41) that simple inhibition of the electrogenic pump has only a small effect on total membrane conductance.

In cells (e.g, the giant algae) where the resting potential is poised nearer the reversal potential for an electrogenic pump, pump switching has a much more pronounced effect on membrane conductance [17, 57]. Contrariwise, in cells where the resting membrane potential is far from the expected reversal potential for the pump (e.g., animal cell membranes with the Na^+/K^+ pump), switching the pump has almost no measurable effect on the membrane conductance [28, 31, 61], a circumstance which

was assumed first by Briggs [7] and later by Moreton [34] in their derivations of the "Constant-Field Equation" with an electrogenic pump.

Maximal current

The maximal current of 18.6–25 $\mu A/cm^2$, which can be driven by the H^+ pump in *Neurospora*, is roughly 200 pmoles/$cm^2 \cdot$ sec, comparable with pumping rates of many specialized transport epithelia [11, 22, 24, 65]. This, alone, signals a major role for the electrogenic pump in cellular economy. More specifically, at a resting membrane potential of -175 mV, the pump current would be 14–19 $\mu A/cm^2$, which implies a minimal power dissipation of 2.4–3.3 $\mu W/cm^2$ or 0.6–0.8 $\mu cal/cm^2 \cdot$ sec, at 100% efficiency. However, if the pump stoichiometry is assumed to be 2 H^+ ions transported for each ATP molecule split, then 14–19 $\mu A/cm^2$ must correspond to 70–95 pmoles of ATP consumed per $cm^2 \cdot$ sec, which becomes 0.22 – 0.30 mmoles/kg cell water $\cdot$ sec (1 kg cell water = 3.19 $\times 10^6$ cm^2 surface [50]). The average rate of ATP synthesis from oxidative metabolism is about 1.17 mmoles/kg cell water $\cdot$ sec [43], so that 19–26% of the total ATP production would be consumed by the pump. The figure is slightly smaller than one arrived at earlier [50], and is improved in the sense that it now derives from the measured pump current and the nonlinear I–V characteristic of the membrane.

For a pump stoichiometry of 1 H^+/1 ATP, 38–52% of the total ATP production would be consumed by the pump, which strongly implies that only cells in an energy-rich environment could afford 1:1 stoichiometry. This circumstance provides an evolutionary rationale for the variable pump stoichiometry which was proposed above.

The work was supported by RCD Award GM-20164 and Research Grant GM-15858 from the U.S. National Institutes of Health. Purchase of the PDP8/E computer was made possible by Grant GB-39975 from the U.S. National Science Foundation. D.G. and J.W. were supported by fellowships Gr409/2 and Wr377 from the Deutsche Forschungsgemeinschaft; and D.G. and U.-P.H., by travel grants Gr409/5 and Ha712/5, also from the Deutsche Forschungsgemeinschaft. U.-P.H. was awarded a fellowship by the James Hudson Brown Memorial Foundation (Yale University); and W.S.L., a fellowship (AM-46807) from the National Institutes of Health. The authors are indebted to Dr. W.K. Chandler for numerous helpful suggestions throughout the experiments, and to Drs. R.W. Tsien and N.A. Walker for critical reading of the manuscript.

Appendix 1

Estimation of current error arising from use of the linear approximation [Eq. (3)] to calculate nonlinear membrane I–V curves. The fractional error

can be calculated as $f=$[expression (4)$-$expression (3)]/expression (3). Of the two variable parameters, α and β, shunting by distant parts of the cable makes α rather insensitive to variations of membrane conductance during current injection; α can arbitrarily be rewritten as $\alpha=1+k(\beta-1)$, where $k<1$. Substituting this expression into f, writing $v_0+v_1\doteq 2v_0$, and $v_o-v_1\equiv \Delta v$, and discarding the small terms of the denominators, gives

$$f\doteq k\beta(\beta-1)\frac{v_o}{\Delta v}. \tag{10}$$

Probable values of β can be generated from polynomials fitted to the average membrane current-voltage curves in Fig. 5 and Table 2, though the origin for the curves must be translated back to the resting membrane potential (V_m), so that [transforming Eq. (5)] the membrane current in any cell (I_m) is

$$I_m=(a_o+a_1V_m+a_2V_m^2)+(a_1+2a_2V_m)v+a_2v^2. \tag{11}$$

Now, $\beta\equiv r_{m1}/r_{m0}=G_{m0}/G_{m1}$, which can be evaluated from dI_m/dv for v_o and for $v_1=v_o-\Delta v$. Finally,

$$\beta=\frac{(a_1+2a_2V_m)+2a_2v_o}{(a_1+2a_2V_m)+2a_2(v_o-\Delta v)}. \tag{12}$$

Table 2 and the underlying experiments give the following approximate values of terms in Eq. (12). $V_m\doteq -180$ mV; at maximal hyperpolarization $v_o=-120$ mV and $\Delta v=-35$ mV; at maximal depolarization $v_o=180$ mV and $\Delta v=40$ mV. The average value of a_2 is -0.000178, and of a_1 is 0.132. Then $\beta=1.06$ for maximal hyperpolarization and 0.9 for maximal depolarization. From test calculations using the equivalent circuit of Fig. 1*B* and the *I–V* curves of Fig. 5, $k\doteq 0.3$. Equation (10) yields $f\doteq 0.07$ for hyperpolarization and -0.12 for depolarization.

Appendix 2

Nonlinear cable analysis. In practice, the nonlinear analysis for membrane current suggested by Adrian and Marshall [Eq. (3) above] [1] yields very scattered results on *Neurospora* hyphae. We therefore developed another approach which does not require prior calculation and constancy of the longitudinal resistance (r_p) for the lumped cable. Its application is facilitated by having analytic expressions to describe the

input I–V plots (Fig. 3), so those plots were first fitted to third-degree polynomial equations constrained to pass through the origin. (For the examples in Fig. 3, actual coefficients are given in the legend.)

As is illustrated in the *Inset* to Fig. 3, each pair of curves defines three sets of quantities: (i) the input current, $i_{T(0)}=i_T$, required to produce a given voltage displacement in *Cell 0*; (ii) the simultaneous displacement of potential in *Cell 1* (v_1); and (iii) another input current, $i_{T(1)}$, which would give the same voltage displacement as v_1, but in *Cell 0*. The following equations can then be written:

$$i_{m0}=i_{T(0)}-2i_{m1}-2i_a \tag{13-0}$$

$$i_{m1}=i_{T(1)}-2i_a, \tag{13-1}$$

where i_a is the axial current flowing away from *Cell 1*. Substitution of Eq. (13-1) into (13-0) gives

$$i_{m0}=i_{T(0)}-i_{T(1)}-i_{m1} \tag{14-0}$$

and similarly

$$i_{m1}=i_{T(1)}-i_{T(2)}-i_{m2} \tag{14-1}$$

$$i_{mn}=i_{T(n)}-i_{T(n+1)}-i_{m(n+1)}. \tag{14-n}$$

By successive back substitution, taking the limit as $n\to\infty$ (stepping into the origin in Fig. 3), we obtain

$$i_{m0}=i_{T(0)}+2\sum_{j=1}^{\infty} i_{T(j)}(-1)^j. \tag{15}$$

The labor of iteration in using Eq. (15) can be reduced by writing the remaining sum in finite form once j has become large enough (close enough to the origin) so that the input I–V curves are linear.

The validity of this equation is restricted by 3 assumptions: electrical symmetry about *Cell 0*; uniformity, so that each cell along the hypha must have the same electrical characteristics as every other cell at a given membrane potential; and monotonicity, such that there is no interval of negative input resistance.

Equation (15) was used to calculate membrane I–V curves in the earlier experiments reported above; later, it was used to check the adequacy of approximating the nonlinear I–V relations by Eq. 3, as illustrated by the comparison of dashed curves [Eq. (15)] and plotted points [Eq. (3)] in Fig. 4.

Appendix 3

There are a number of circumstances – particularly when non-steady-state events are being considered – when it would be useful to know the approximate shape of the membrane current-voltage curve with the electrogenic pump off or partly off, but when the complete cyanide experiment (Fig. 7) cannot be done. From the set of paired membrane *I–V* curves underlying Fig. 8, a remarkable empirical relationship emerged, *viz.*, that the slope of the membrane *I–V* curve in the presence of cyanide is approximately proportional, at all voltages, to the slope of the control *I–V* curve. Provided that two points on the inhibited *I–V* curve can be specified, the entire curve can then be calculated. One known point is the actual membrane potential in cyanide, which is designated $V_{m0}(t)$ in Eq. (7), and will be abbreviated V_{CN} here; the other point is E_p, where (by definition) the two curves intersect. Then the membrane current in cyanide (I_{CN}) is given by

$$I_{CN}=\frac{I_{m0}(E_p)}{I_{m0}(E_p)-I_{m0}(V_{CN})}[I_{m0}-I_{m0}(V_{CN})], \tag{16}$$

where $I_{m0}(\ )$ means "I_{m0} evaluated at ...," and I_{m0} is given by Eq. (5) with the quadratic coefficients specified for the control *I–V* curve, without cyanide.

One example of an *I–V* relationship calculated in this manner is shown by the dashed curve in Fig. 7. While deviations from the plotted points or from the fitted polynomial (solid curve) are clear in this case, they were not systematic from one case to the next. And for the average of all nine cases, I_{CN} calculated by Eq. (16) was completely superimposable on the plotted points, except at membrane potentials positive to −40 mV, where Eq. (16) rose systematically above the points. The average scaling factor relating I_{CN} to I_{m0} was 0.82. In these calculations, best results were obtained using optimized values of E_p, which averaged −418 mV, 28 mV beyond E_p estimated in Fig. 9.

Equation (16) can be put to two immediate purposes: to estimate total pump *I–V* curves, as if cyanide switched the pump completely off; and to calculate the expected time course of conductance change at the onset of cyanide inhibition. The pump *I–V* curve can be calculated from Eq. (16) as $I_{pump}=I_{m0}-I_{CN}$. A reasonable estimate of the total membrane diffusion potential from a variety of experiments [41, 42, 50] is about −25 mV, which should be observed (on average) with the pump completely off. When the average I_{pump} curve is calculated with this value

of I_{CN} and is divided by the curve calculated with the observed average potential (Table 3) in cyanide, -73 mV, a ratio of 1.3 is obtained, indicating that 23% of the normal pump current still flows during maximal cyanide inhibition. Hence, the rough figure of 25% given in the discussion of Fig. 9. For the time-course of conductance change at the onset of cyanide inhibition, we differentiate Eq. (16) with respect to V_{CN} to obtain Eq. (7). That equation can then be fitted to the combined conductance and voltage data (Fig. 10) as described in the text.

References

1. Adrian, R.H., Marshall, M.W. 1977. Sodium currents in mammalian muscle. *J. Physiol. (London)* **268**:223
2. Adrian, R.H., Slayman, C.L. 1966. Membrane potential and conductance during transport of sodium, potassium, and rubidium in frog muscle. *J. Physiol. (London)* **184**:970
3. Alberty, R.A. 1968. Effect of pH and metal ion concentration on the equilibrium hydrolysis of adenosine triphosphate to adenosine diphosphate. *J. Biol. Chem.* **243**:1337
4. Benz, R., Stark, G. 1975. Kinetics of macrotetrolide-induced ion transport across lipid bilayer membranes. *Biochim. Biophys. Acta* **382**:27
5. Blankemeyer, J.T., Harvey, W.R. 1977. Insect midgut as a model epithelium. *In:* Water Relations in Membrane Transport in Plants and Animals. A.M. Jungreis, T.K. Hodges, A. Kleinzeller, and S.G. Schultz, editors. pp. 161–182. Academic Press, New York
6. Bowman, B.J., Slayman, C.W. 1977. Characterization of plasma membrane adenosine triphosphatase of *Neurospora crassa*. *J. Biol. Chem.* **252**:3357
7. Briggs, G.E. 1962. Membrane potential differences in *Chara australis*. *Proc. R. Soc. London B* **156**:573
8. Chapman, J.B., Johnson, E.A. 1976. Current-voltage relationships for theoretical electrogenic sodium pump models. *Proc. Aust. Physiol. Pharmacol. Soc.* **7**:69P
9. Coster, H.G.L. 1969. The role of pH in the punch-through effect in the electrical characteristics of *Chara australis*. *Aust. J. Biol. Sci.* **22**:365
10. Coster, H.G.L., Smith, J.R. 1974. The effect of pH on the low frequency capacitance of the membranes of *Chara corallina*. *In:* Membrane Transport in Plants. U. Zimmermann and J. Dainty, editors. pp. 154–161. Springer-Verlag, Berlin
11. Crane, E.E., Davies, R.E., Longmuir, N.M. 1948. Relations between hydrochloric acid secretion and electrical phenomena in frog gastric mucosa. *Biochem. J.* **43**:321
12. Cross, S.B., Keynes, R.D., Rybová, R. 1965. The coupling of sodium efflux and potassium influx in frog muscle. *J. Physiol. (London)* **181**:865
13. Dainty, J., Lannoye, R.J., Tarr, S.E. 1970. Voltage-current characteristics of *Chara australis* during changes of pH and exchange of Ca-Mg in external medium. *J. Exp. Bot.* **21**:558
14. Dilley, R.A., Giaquinta, R.T. 1975. H^+ ion transport and energy transduction in chloroplasts. *Curr. Top. Membr. Transp.* **7**:49
15. Finkelstein, A. 1964. Carrier model for active transport of ions across a mosaic membrane. *Biophys. J.* **4**:421

16. Forte, J.G. 1971. Hydrochloric acid secretion by gastric mucosa. *In:* Membranes and Ion Transport. E.E. Bittar, editor. Vol. 3, p. 111, Wiley Interscience, New York
17. Gradmann, D. 1975. Analog circuit of the *Acetabularia* membrane. *J. Membrane Biol.* **25**:183
18. Gradmann, D., Slayman, C.L. 1975. Oscillations of an electrogenic pump in the plasma membrane of *Neurospora. J. Membrane Biol.* **23**:181
19. Hanstein, W.G. 1976. Uncoupling of oxidative phosphorylation. *Biochim. Biophys. Acta* **456**:129
20. Harold, F.M. 1977. Membranes and energy transduction in bacteria. *Curr. Top. Bioenerg.* **6**:83
21. Haydon, D.A., Hladky, S.B. 1972. Ion transport across thin lipid membranes: A critical discussion of mechanisms in selected systems. *Q. Rev. Biophys.* **5**:187
22. Helman, S.I., Fisher, R.S. 1977. Microelectrode studies of the active Na transport pathway of frog skin. *J. Gen. Physiol.* **69**:571
23. Higinbotham, N. 1973. Electropotentials of plant cells. *Annu. Rev. Plant Physiol.* **24**:25
24. Hill, A.E. 1967. Ion and water transport in *Limonium.* II. Short-circuit analysis. *Biochim. Biophys. Acta* **135**:461
25. Hunsley, D., Gooday, G.W. 1974. The structure and development of septa in *Neurospora crassa. Protoplasma* **82**:125
26. Kayalar, C., Rosing, J., Boyer, P.D. 1976. 2,4-Dinitrophenol causes a marked increase in the apparent K_m of P_i and ADP for oxidative phosphorylation. *Biochim. Biophys. Res. Commun.* **72**:1153
27. Komor, E., Tanner, W. 1974. The hexose-proton cotransport system in *Chlorella. J. Gen. Physiol.* **64**:568
28. Lambert, J.D.C., Kerkut, G.A., Walker, R.J. 1974. The electrogenic sodium pump and membrane potential of identified neurons in *Helix aspersa. Comp. Biochem. Physiol.* **47A**:897
29. Lambowitz, A.M., Slayman, C.W. 1971. Cyanide-resistant respiration in *Neurospora crassa. J. Bacteriol.* **108**:1087
30. Mandel, L.J., Curran, P.F. 1973. Response of the frog skin to steady-state voltage clamping. II. The active pathway. *J. Gen. Physiol.* **62**:1
31. Marmor, M.F. 1971. The independence of electrogenic sodium transport and membrane potential in a molluscan neurone. *J. Physiol. (London)* **218**:599
32. Marquardt, D.W. 1963. An algorithm for least-squares estimation of non-linear parameters. *J. Soc. Ind. Appl. Math.* **11**:431
33. Mitchell, P. 1963. Molecule, group and electron translocation through natural membranes. *Biochem. Soc. Symp.* **22**:142
34. Moreton, R.B. 1969. An investigation of the electrogenic sodium pump in snail neurones, using the constant field theory. *J. Exp. Biol.* **51**:181
35. Ramos, S., Kaback, H.R. 1977. The relationship between the electrochemical proton gradient and active transport in *Escherichia coli* membrane vesicles. *Biochemistry* **16**:854
36. Ritchie, J.M. 1971. Electrogenic ion pumping in nervous tissue. *Curr. Top. Bioenerg.* **4**:327
37. Scarborough, G.A. 1977. Properties of the *Neurospora crassa* plasma membrane ATPase. *Arch. Biochem. Biophys.* **180**:384
38. Skulachev, V.P. 1974. Mitochondrial adenosine triphosphatase, cytochrome *c* oxidase, and bacteriorhodopsin as biological electric generators. *In:* Membrane Adenosine Triphosphatases and Transport Processes. J.R. Bronk, editor. p. 175. Biochemical Society, London

39. Skulachev, V.P. 1977. Transmembrane electrochemical H^+-potential as a convertible energy source for the living cell. *FEBS Lett.* **74**:1
40. Slayman, C.L. 1965. Electrical properties of *Neurospora crassa.* Effects of external cations on the intracellular potential. *J. Gen. Physiol.* **49**:69
41. Slayman, C.L. 1965. Electrical properties of *Neurospora crassa:* Respiration and the intracellular potential. *J. Gen. Physiol.* **49**:93
42. Slayman, C.L. 1970. Movement of ions and electrogenesis in microorganisms. *Am. Zool.* **10**:377
43. Slayman, C.L. 1973. Adenine nucleotide levels in *Neurospora,* as influenced by conditions of growth and by metabolic inhibitors. *J. Bacteriol.* **114**:752
44. Slayman, C.L. 1974. Proton pumping and generalized energetics of transport: A review. *In:* Membrane Transport in Plants. U. Zimmermann and J. Dainty, editors. p. 107. Springer-Verlag, Berlin
45. Slayman, C.L. 1977. Energetics and control of transport in *Neurospora. In:* Water Relations in Membrane Transport in Plants and Animals. A.M. Jungreis, T.K. Hodges, A. Kleinzeller and S.G. Schultz, editors. p. 69. Academic Press, New York
46. Slayman, C.L., Gradmann, D. 1973. The equivalent circuit for a membrane with an electrogenic pump. *Abstr. Biophys. Soc. Meeting,* Item TAM-J10
47. Slayman, C.L., Gradmann, D. 1975. Electrogenic proton transport in the plasma membrane of *Neurospora. Biophys. J.* **15**:968
48. Slayman, C.L., Gradmann, D., Hansen, U.-P. 1976. Electrophysiological aspects of energy transfer in the plasma membrane of *Neurospora. In:* Semaine d'Étude sur le Thème Membranes Biologiques et Artificielles et la Désalinisation de l'Eau. R. Passino, editor. p. 403. Pontificial Academy of Sciences, Rome
49. Slayman, C.L., Long, W.S., Gradmann, D. 1976. "Action potentials" in *Neurospora crassa,* a mycelial fungus. *Biochim. Biophys. Acta* **426**:732
50. Slayman, C.L., Long, W.S., Lu, C.Y.-H. 1973. The relationship between ATP and an electrogenic pump in the plasma membrane of *Neurospora crassa. J. Membrane Biol.* **14**:305
51. Slayman, C.L., Lu, C.Y.-H., Shane, L. 1970. Correlated changes in membrane potential and ATP concentrations in *Neurospora. Nature (London)* **226**:274
52. Slayman, C.L., Slayman, C.W. 1968. Net uptake of potassium in *Neurospora:* Exchange for sodium and hydrogen ions. *J. Gen. Physiol.* **52**:424
53. Slayman, C.L., Slayman, C.W. 1974. Depolarization of the plasma membrane of *Neurospora* during active transport of glucose: Evidence for a proton-dependent cotransport system. *Proc. Nat. Acad. Sci. USA* **71**:1935
54. Slayman, C.L., Slayman, C.W., Hansen, U.-P. 1977. Current-voltage relationships for the glucose/H^+ cotransport system in *Neurospora. In:* Transmembrane Ionic Exchanges in Plants. M. Thellier and A. Monnier, editors. C.N.R.S., Paris (*in press*)
55. Slayman, C.W., Rees, D.C., Orchard, P.P., Slayman, C.L. 1975. Generation of adenosine triphosphate in cytochrome-deficient mutants of *Neurospora. J. Biol. Chem.* **250**:396
56. Slayman, C.W., Slayman, C.L. 1975. Energy coupling in the plasma membrane of *Neurospora*: ATP-dependent proton transport and proton-dependent sugar cotransport. *In:* Molecular Aspects of Membrane Phenomena. H.R. Kaback, H. Neurath, G.K. Radda, R. Schwyzer, and W.R. Wiley, editors. p. 233. Springer-Verlag, Berlin
57. Spanswick, R.M. 1972. Evidence for an electrogenic ion pump in *Nitella translucens.* I. The effects of pH, K^+, Na^+, light and temperature on the membrane potential and resistance. *Biochim. Biophys. Acta* **288**:73
58. Stark, G. 1973. Rectification phenomena in carrier-mediated ion transport. *Biochim. Biophys. Acta* **298**:323

59. Stark, G., Benz, R. 1971. The transport of potassium through lipid bilayer membranes by the neutral carriers valinomycin and monactin. Experimental studies to a previously proposed model. *J. Membrane Biol.* **5**:133
60. Thayer, W.S., Hinkle, P.C. 1973. Stoichiometry of adenosine triphosphate-driven proton translocation in bovine heart submitochondrial particles. *J. Biol. Chem.* **248**:5395
61. Thomas, R.C. 1969. Membrane current and intracellular sodium changes in a snail neurone during extrusion of injected sodium. *J. Physiol. (London)* **201**:495
62. Thomas, R.C. 1972. Electrogenic sodium pump in nerve and muscle cells. *Physiol. Rev.* **52**:563
63. Trinci, A.P.J., Collinge, A.J. 1974. Occlusion of the septal pores of damaged hyphae of *Neurospora crassa* by hexagonal crystals. *Protoplasma* **80**:57
64. Tsuda, S., Tatum, E.L. 1961. Intracellular crystalline ergosterol in *Neurospora. J. Biophys. Biochem. Cytol.* **11**:171
65. Ussing, H.H., Zerahn, K. 1951. Active transport of sodium as the source of electric current in the short-circuited isolated frog skin. *Acta Physiol. Scand.* **23**:100
66. Vogel, H.J. 1956. A convenient growth medium for *Neurospora* (Medium N). *Microbial Gen. Bull.* **13**:42